ENVIRONMENTAL RESEARCH
LETTERS

LETTER • OPEN ACCESS

A multivariate probabilistic framework for tracking the regional tropical edges: analysis of inter-annual variations and long-term trends

ENVIRONMENTAL RESEARCH
LETTERS

CrossMark

OPEN ACCESS

RECEIVED
11 December 2023

REVISED
21 March 2024

ACCEPTED FOR PUBLICATION
5 April 2024

PUBLISHED
19 April 2024

LETTER

A multivariate probabilistic framework for tracking the regional tropical edges: analysis of inter-annual variations and long-term trends

Xinxian Feng[1,3], Weichen Tao[1,*], Gang Huang[1,2,3,*], Yongyun Hu[4], William K M Lau[5], Xia Qu[1,6], Kaiming Hu[1,6] and Ya Wang[1]

1 State Key Laboratory of Numerical Modeling for Atmospheric Sciences and Geophysical Fluid Dynamics, Institute of Atmospheric Physics, Chinese Academy of Sciences, Beijing 100029, People's Republic of China
2 Laboratory for Regional Oceanography and Numerical Modeling, Qingdao National Laboratory for Marine Science and Technology, Qingdao 266237, People's Republic of China
3 University of Chinese Academy of Sciences, Beijing 100049, People's Republic of China
4 Laboratory for Climate and Ocean–Atmosphere Studies, Department of Atmospheric and Oceanic Sciences, School of Physics, Peking University, Beijing 100871, People's Republic of China
5 Earth System Science Interdisciplinary Center, University of Maryland, College Park, MD 20740, United States of America
6 Center for Monsoon System Research, Institute of Atmospheric Physics, Chinese Academy of Sciences, Beijing 100029, People's Republic of China
* Authors to whom any correspondence should be addressed.

E-mail: tao@mail.iap.ac.cn and hg@mail.iap.ac.cn

Keywords: regional tropical edge, Hadley circulation, tropical belt, multivariate probabilistic framework, copula function

Supplementary material for this article is available online

Abstract

In the present study, a multivariate probabilistic framework is used to identify the meridional positions of regional tropical edges (RTEs), which are based on two variables: sea level pressure and precipitation minus evaporation. This new defined metric effectively captures inter-annual variability and long-term trend of the commonly adopted zonal mean tropical edge based on meridional mass stream function and near-surface winds. Besides, pronounced RTE trends are primarily located over the oceanic regions, and the terrestrial areas exhibit substantial inter-annual variability. These results are consistent among three modern reanalysis datasets. Moreover, the impacts of climate modes on RTE are investigated. The El Niño-Southern Oscillation, the Atlantic multi-decadal oscillation, and the Southern Annular Mode are important both on the inter-annual variations and long-term trends of RTE. The Pacific Decadal Oscillation is more inclined to affect long-term contribution rather than inter-annual relationship, and the Pacific–North American teleconnection, the North Atlantic Oscillation, and the Arctic oscillation highlight the inter-annual relationship with RTE in the specific regions, such as North Pacific, North Atlantic, and North Africa, respectively.

1. Introduction

The tropical belt is the region manifested by the Hadley circulation, with updraft and intense rainfall near the equator, as well as downdraft and arid zones in the subtropics of each hemisphere. In the past few decades, numerous studies have utilized observations and reanalysis data to discover the tropical expansion trend since the late 1970s (Fu *et al* 2006, Hu and Fu 2007, Seidel *et al* 2007, Seidel and Randel 2007, Fu and Lin 2011, Davis and Rosenlof 2012, Allen *et al* 2014, Davis and Davis 2018, Grise *et al* 2018, 2019, Ma *et al* 2018, Staten *et al* 2018, Lau and Tao 2020), accompanied by the poleward shift of the subtropical jet, subtropical high, and sinking branch of the Hadley circulation (Fu *et al* 2006, Archer and Caldeira 2008, Fu and Lin 2011, Grise *et al* 2018), as well as the poleward movement of subtropical arid zone (Dai 2011, Cai *et al* 2012, Allen *et al* 2014, He and Soden 2016, Huang *et al* 2016, 2017, Tivig *et al* 2020). However, the poleward shift of the tropical edge is unlikely to occur at all longitudes and exhibits significant regional features

(Nguyen *et al* 2017, Grise *et al* 2018, Staten *et al* 2020). Additionally, from the perspective of climatology, the contribution of regional Hadley circulation to zonal mean Hadley circulation also varies with region. For example, taking the tropical zonal wind field as an example, its intensity varies in different regions, and even the northerly winds appear in some regions (Hoskins *et al* 2020, Hoskins and Yang 2021).

Previous studies have pointed out that tropical expansion can cause a series of regional climate changes in the subtropics, such as shifting the dry zones (Feng and Fu 2013, Schmidt and Grise 2017), altering the regions of oceanic upwelling (Rykaczewski *et al* 2015), modifying typhoon tracks (Kossin *et al* 2014, Rykaczewski *et al* 2015, Sharmila and Walsh 2018, Studholme and Gulev 2018, Anjana and Kumar 2023), and exacerbating wildfires (Zhang *et al* 2020). The changes of regional tropical edges (RTEs) may serve an important role in linking tropical expansion and regional climate impacts.

At present, there are still limited studies on the changes of RTE, owing to the difficulty in defining the RTE. Previous studies have made some attempts, but more works are needed. Chen *et al* (2014) selected six regions globally and studied the long-term trends of tropical edges in these regions by using an outward longwave radiation (OLR) based metric. Their results showed that the expansion was more obvious in the Northern Hemisphere (NH) than the Southern Hemisphere (SH), with a greater contribution from the eastern Pacific. However, the OLR based metric strongly depends on the selection of thresholds (Davis and Rosenlof 2012, Nguyen *et al* 2017), and OLR is not only affected by atmospheric circulation dynamics but also related to atmospheric thermal properties (Waugh *et al* 2018), leading to the considerable uncertainty in the obtained results. In addition, Schwendike *et al* (2015) attempted to use the improved mass stream function by applying the meridional component of the divergent winds instead of the conventional meridional winds at each longitude and examined the RTE at 500 hPa. According to this metric, the inter-annual variability of RTE over the Asia–Pacific sector dominantly governs that of the tropical edge in the SH (Nguyen *et al* 2017), and the long-term trend over the eastern Pacific showed the largest contribution in the recent tropical expansion (Staten *et al* 2019). Due to the use of mass stream function, this metric captures the dynamic characteristics of RTE and its close relationship with near-surface climate. However, on one hand, it is not clear whether this metric can be a true representation of the RTE (Hu *et al* 2018). On the other hand, the obtained edges are not continuous over the entire latitude circle and cannot represent the changes in certain specific regions. For the metric by using sea level pressure (SLP), the long-term changes of RTE were found to be mainly located in oceans, and the SLP based metric could not reflect edge changes on land (Schmidt and Grise 2017). Moreover, the results of the above three metrics in each region are not completely consistent (Chen *et al* 2014, Schmidt and Grise 2017, Staten *et al* 2019), indicating that the single metric has strong metric dependency.

Therefore, it is necessary to select more suitable variables and develop new metrics for better representing the location of RTE and exploring the possible influencing factors for RTE variations. The rest of the text is organized as follows: section 2 provides data and methods. Section 3 provides the main results, including the inter-annual variations and long-term trends of the new defined multivariate metric at zonal mean and regional scale, as well as the potential influence of climate modes on RTE. Section 4 provides a concluding summary.

2. Data and methods

2.1. Data

Due to the diverse performance of reanalysis datasets in depicting the variations of the Hadley circulation (Allan and Soden 2007, Stachnik and Schumacher 2011, Nguyen *et al* 2013, Davis and Birner 2017, Davis and Davis 2018, Grise *et al* 2018, Lau and Tao 2020), and modern reanalyses can better capture the tropical expansion characteristics (Grise *et al* 2019). Therefore, monthly mean output for the period of 1979–2020 from three modern reanalyses are used in this study: fifth generation of European Centre for Medium-Range Weather Forecasts (ECMWF) atmospheric reanalyses of the global climate (ERA5; Hersbach *et al* 2020), the National Aeronautics and Space Administration's Modern-Era Retrospective Analysis for Research and Applications 2 (MERRA2; Gelaro *et al* 2017), the Japanese Meteorological Agency's Japanese 55 year Reanalysis (JRA55; Kobayashi *et al* 2015). In the main body of this paper, the primary conclusions are drawn from ERA5, which has the highest resolution. The other two reanalysis datasets are employed for validation purposes, and the relevant results are shown in supplemental materials.

2.2. Methods

2.2.1. Metrics measuring the zonal mean tropical edge

From the perspective of zonal mean, there are various metrics to measure the meridional position of the tropical edge. The most used metrics are defined according to the position of vertical descent in the mid-layers of the troposphere between the Hadley circulation and Ferrel circulation, specifically the zero-crossing of meridional mass stream function in the subtropics at 500 hPa (PSI metric; Hu and Fu 2007), which holds clear dynamical implication.

The other metrics can be categorized into upper-atmospheric and lower-atmospheric metrics. Upper-atmospheric metrics include the latitude where OLR equals 250 W m^{-2} (Hu and Fu 2007) and the position of the tropopause break (Davis and Rosenlof 2012, Xian and Homeyer 2019). Lower-atmospheric metrics include the position where precipitation minus evaporation firstly reaches minimal or zero (PE metric; Lu *et al* 2008, Davis and Birner 2017), the latitude of maximum SLP (SLP metric; Hu *et al* 2010, Choi *et al* 2014), the latitude where the near-surface winds become westerlies (UAS metric; Davis and Birner 2017, Grise and Davis 2020), and the latitude of eddy-driven jet (EDJ metric; Schneider 2006, Kang and Polvani 2011). Compared to the upper-atmospheric metrics, lower-atmospheric metrics more effectively capture the inter-annual variations and long-term trends of the PSI metric (Solomon *et al* 2016, Davis and Birner 2017, Waugh *et al* 2018). This is mainly due to the fact that lower-atmospheric metrics are more readily constrained by the momentum transport associated with the Hadley circulation, while upper-atmospheric metrics reside in the free atmosphere and primarily follow thermal wind relationships (Grise *et al* 2019, Staten *et al* 2020). Moreover, Waugh *et al* (2018) mentioned the forced response of the EDJ metric may substantially differ from direct measures of tropical width, such as the PSI metric. Thus, the present study primarily focuses on the rest three lower-atmospheric metrics based on PE, SLP and UAS.

The computational modules for zonal mean tropical edge calculations are derived from the Tropical-width Diagnostics software package (Adam *et al* 2018). These modules encompass functionalities dedicated to the determination of latitudinal points where zero-crossings, thresholds, and maxima of variables are satisfied. The statistical methods including the regression and correlation analysis are used in sections 3.1 and 3.2 to investigate the inter-annual and long-term characteristics of the new defined metric, while the partial regression and partial correlation analysis are used in section 3.3 to explore the influence of climate modes on RTE. The significance level is estimated based on the standard two-tailed Student's t-test.

2.2.2. A multivariate probabilistic framework

In the present study, we applied a multivariate probabilistic framework, which was first proposed by Mamalakis and Foufoula-Georgiou (2018) to precisely identify the regional features of the intertropical convergence zone. The framework relies upon statistical copula models, employing mathematical methods to access multiple variables simultaneously. The movement of the tropical edge is accompanied by the adjustments of various variables (Allen *et al* 2012, 2014, Birner *et al* 2014, Brönnimann *et al* 2015, Lau and Kim 2015, Lau and Tao 2020), and this method provides a more comprehensive approach to consider the interactions between different variables at fine-scale.

Based on Mamalakis and Foufoula-Georgiou (2018) and Mamalakis *et al* (2021), the location of the RTE at a longitude l under the multivariate probabilistic framework can be obtained through the following steps:

(1) Select N variables (in this study, $N = 2$), and calculate annual average of these variables. Take a latitudinal window ($[l - w/2, l + w/2]$, where w is the window width, and $w = 15°$ in this study, consistent with the latitudinal window width used in Choi *et al* (2014) and Totz *et al* (2018). The zonal average of N variables is calculated within this window.
(2) Compute the copula function for the N variables longitudinally during the year t ($t = 1979, 1980, 1981, \ldots, 2020$).
(3) Calculate the cumulative distribution function (CDF) of the copula function, and the latitude where its CDF exceeds a certain threshold a (in this study, $a = 70\%$) is considered as the position of the RTE for that specific longitude l and year t. Noted that this result corresponds to the latitude where maximum SLP and minimum PE occur simultaneously.

Utilizing this framework, we can develop a new metric that considers the physical relationship among two or more variables simultaneously. Additionally, by varying the parameters w, N, and a, the sensitivity of the results for different problem scenarios could be tested. Note that the obtained position of the RTE exhibits a limited sensitivity to parameter selection. Slight adjustments to the parameters of w and a only influence the specific numerical values of the CDF and do not alter the major conclusions of the present study.

2.2.3. Selection of variables for RTE

Consistent with the zonal mean tropical edge, the location of RTE should be close to the areas that correspond with the downdraft and the arid zone (Staten *et al* 2019). Therefore, among the three lower-atmospheric variables, a metric defined under the multivariate probabilistic framework to reasonably delineate the RTE is enabled: (1) the variable should well capture the maximum downward movements, as the minimum of PE (Davis and Birner 2017); (2) the variable should have a connection with the aridity, as the maximum SLP (Lau and Kim 2015).

A more informed selection process to discern the disparities of the three lower-atmosphere metrics is shown in figure 1(a), which presents the climatological spatial distribution of RTE based on PE, SLP, and UAS metric. The maximum SLP and minimum PE at each longitude have almost identical latitude differences of approximately 10°, and show the apparent

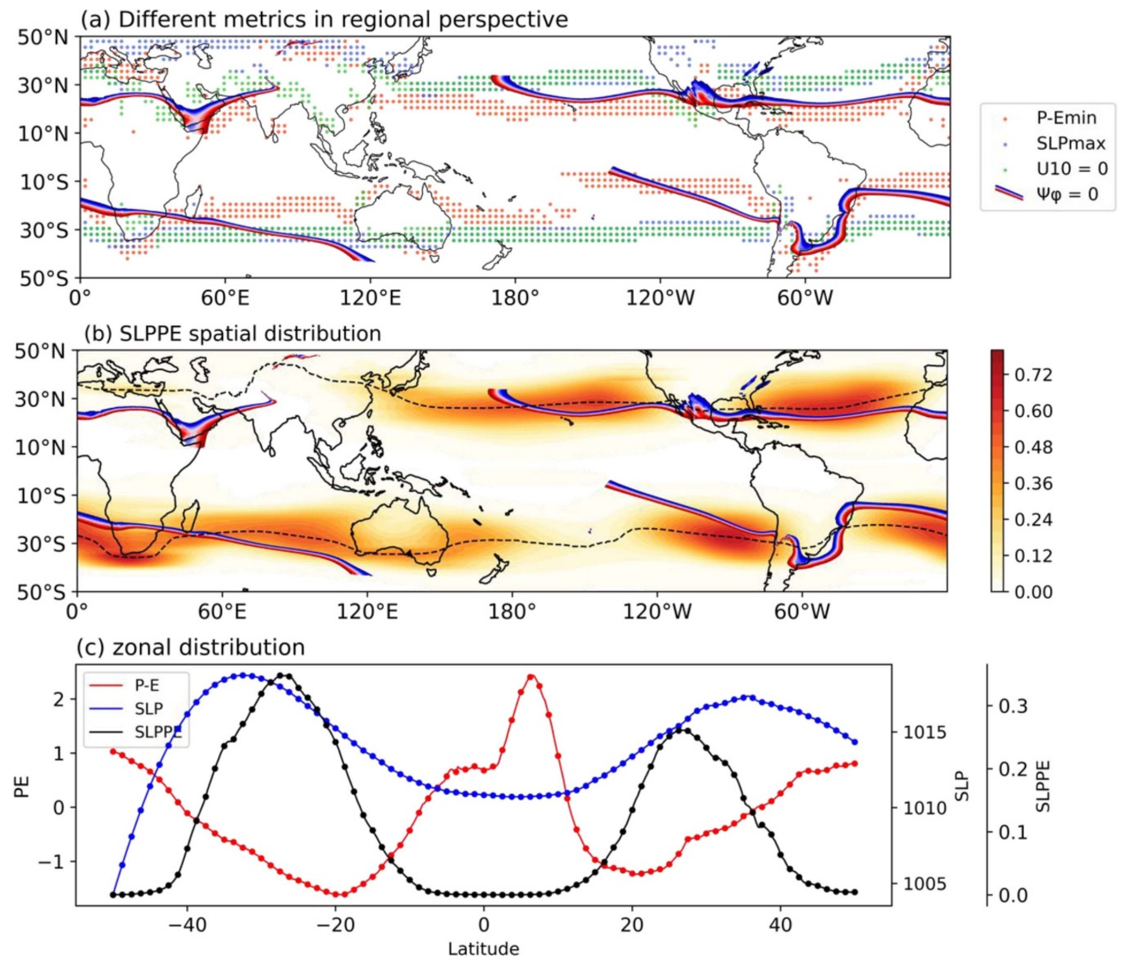

Figure 1. (a) Climatological spatial distribution of RTE based on $\Psi\varphi$, PE, SLP, and UAS metric spanning the period from 1979 to 2020, represented by the zero-crossing areas of 500 hPa $\Psi\varphi$ (shading from red to blue indicates from positive value to negative one), areas of bottom 10% PE (red dots), areas of top 10% SLP (blue dots), and the areas of zero-crossing point with $\pm 2.5°$ deviation of near-surface winds in the transition from easterlies to westerlies (green dots). (b) Spatial distribution of climatological joint CDF between SLP and PE spanning the period from 1979 to 2020 (shading). The black dotted line demarcates the position of the maximum joint CDF between SLP and PE. (c) Zonal mean of PE (red line), SLP (blue line), and SLPPE (black line).

larger meridional differences over Central and West Asia and Australia. For maximum SLP, some high outliers are observed over North America and Central Eurasia, accompanied by high pressure caused by sea–land thermal difference. Compared with maximum SLP, minimum PE tend to locate more equatorward. Note that although the spatial distribution of the zero-crossing of UAS roughly matches with that of maximum SLP, large differences can be observed over the North American and Asian monsoon regions with the other two metrics. Moreover, the definition of UAS metric derived from the balance between the vertically averaged eddy momentum flux convergence and surface drag on the zonal mean surface zonal wind (Davis and Birner 2017), but their regional-scale implications remain ambiguously. Thus, SLP and PE are used to construct the multivariate RTE metric, which is denoted as the SLPPE metric.

For comparison, the metric based on horizontally divergent winds is used (Keyser *et al* 1989, Schwendike *et al* 2015, Staten *et al* 2019), and the overturning stream function at each longitude is calculated as:

$$\Psi\varphi = \frac{2\pi\, a\cos\varphi}{g}\int_0^p V_{\mathrm{d}}\,\mathrm{d}p,$$

where V_{d} is the meridional component of the divergent winds calculated by Helmholtz decomposition, a is the radius of Earth, and g is the gravitational acceleration. Consistent with previous results, the RTE obtained by the $\Psi\varphi$ at 500 hPa are not latitudinally continuous and located between the maximum SLP and the minimum PE at most longitudes (figure 1(a)), further supporting the reasonable selection of these two variables.

The climatological joint CDF between SLP and PE is shown in figure 1(b), generally encompassing the RTE obtained by $\Psi\varphi$ metric. This characteristic is further reproduced in MERRA2 and JRA55 (figure S1 in the supplemental material). Additionally, the RTE depicted by SLPPE are located between the maximum

SLP and minimum PE both at regional (figures 1(a) and (b)) and zonal mean scale (figure 1(c)), and the high CDF values between SLP and PE correspond well with the maximum SLP and minimum PE (figure S2 in the supplemental material), indicating that the SLPPE metric effectively considers both of them. The advantage of SLPPE metric is that it not only allows to cover the location of RTE represented by the divergent winds but also the location where the divergent winds are not well determined.

3. Results

3.1. Inter-annual variability and long-term trend of zonal mean edge

The reliability of the positions of RTE based on SLPPE metric under the probabilistic framework is first inspected for its consistency with the conclusions drawn from previous studies concerning zonal mean metrics at both inter-annual and long-term timescale. Considering the variables used for the copulas function, it is reasonable to infer the RTE defined by SLPPE metric exhibit a strong correlation with SLP and PE. Figures 2(a) and (b) show the time series of zonal mean positions of RTE based on the SLPPE metric, compared with the time series of positions of tropical edge based on the four zonal mean metrics based on PSI, PE, SLP, and UAS in the NH and SH, respectively. The temporal evolution of the SLPPE metric shares a similar inter-annual variation feature with the four zonal mean metrics both in the NH and SH. In particular, the correlation coefficients between the SLPPE metric and the four metrics exceed 0.42 except for the PSI metric in the NH (figure 2(c)), reaching the 99% confidence level. The lowest correlation coefficient between the SLPPE metric and PSI metric in the NH stands at 0.34, which is still significant at the 95% confidence level.

Besides, the poleward shifts of the tropical edge are observed both in the NH and SH (figures 2(a), (b) and (d)). In the SH, the expansion trend is remarkably consistent in all metrics, at approximately 0.2 degrees per decade. However, in the NH, there is a larger discrepancy of trends among metrics. The long-term trends of PSI and SLP metric exhibit comparatively weaker tendencies, whereas more significant tropical expansion trends can be seen in PE and UAS (Baldassare *et al* 2023). The trends of the SLPPE metric are notably stronger in both hemispheres compared to the other four metrics. This phenomenon may arise from the methodology employed for its calculation, due to that the time series of the SLPPE metric involves regional calculations first and then the zonal mean calculations, potentially excessively emphasizing the trends within certain regions. The time series of the SLPPE metric based on JRA55 and MERRA2 closely resemble those from ERA5, with correlation coefficients exceeding 0.7 both in the NH and SH (figure S3 in the supplemental material). Therefore, the SLPPE metric well captures the inter-annual variability and long-term trend of zonal mean tropical edge based on the four zonal mean metrics, and the inter-annual variability and long-term trend of RTE are further investigated in the next subsection.

3.2. Inter-annual variability and long-term trend at regional scale

Figure 3(a) shows the climatology and linear trend of joint CDF between SLP and PE from 1979 to 2020, and figures 3(b) and (c) present the inter-annual variations and long-term trends of RTE in the NH and SH, respectively. In the NH, significant poleward shifts of RTE are observed over the North Pacific and North Atlantic at about 0.3°–0.6° per decade and with relatively low inter-annual variability (figure 3(b)), accompanied by the anomalous decreasing and increasing trends of CDF in the south and north of the climatological RTE, respectively (figure 3(a)). Due to the strong inter-annual variability of terrestrial RTE, the long-term trends in most regions of Eurasia and North America are not significant. Consistent with the recent weakening intensity of the monsoon and the expansion of the transition zone (Dabang and Huijun 2005, Zhang and Zhou 2015, Wang *et al* 2016, Seth *et al* 2019), the RTE in East Asia shows some poleward trends, although the trends in most regions do not reach the confidence level (figures 3(a) and (b)).

In the SH, the most pronounced poleward trends of RTE can be seen over the South Pacific, South Atlantic, South Africa, and southeastern Australia, at approximately 0.4°–0.7° per decade (figure 3(c)), contributing to the drying trend of SH semi-arid regions (Cai *et al* 2012). Note that the trends are not significant over 170° W–130° W of South Pacific due to the vigorous inter-annual variations (figure 3(c)). The poleward trend is around 0.15° per decade over the South Indian Ocean. Similar to the RTE trend over North America, the RTE in South America also tends to move equatorward with strong inter-annual variability (figures 3(b) and (c)).

The RTE expansion over the central and eastern Pacific in the NH and SH are consistent with the results obtained by using $\Psi\varphi$ (Staten *et al* 2019) and OLR metric (Chen *et al* 2014), and the poleward shift of RTE over the Atlantic in both hemispheres are also seen in the RTE trends of SLP metric (Schmidt and Grise 2017). Generally, the pronounced RTE trends are primarily located over the oceanic regions (Schmidt and Grise 2017), while the terrestrial areas exhibit substantial inter-annual variability. Furthermore, the spatial distribution depicting the linear trend of joint CDF between SLP and PE from JRA55 and MERRA2 are further inspected in the supplemental figure S4. The CDF trends from JRA55 and MERRA2 are highly close to those from

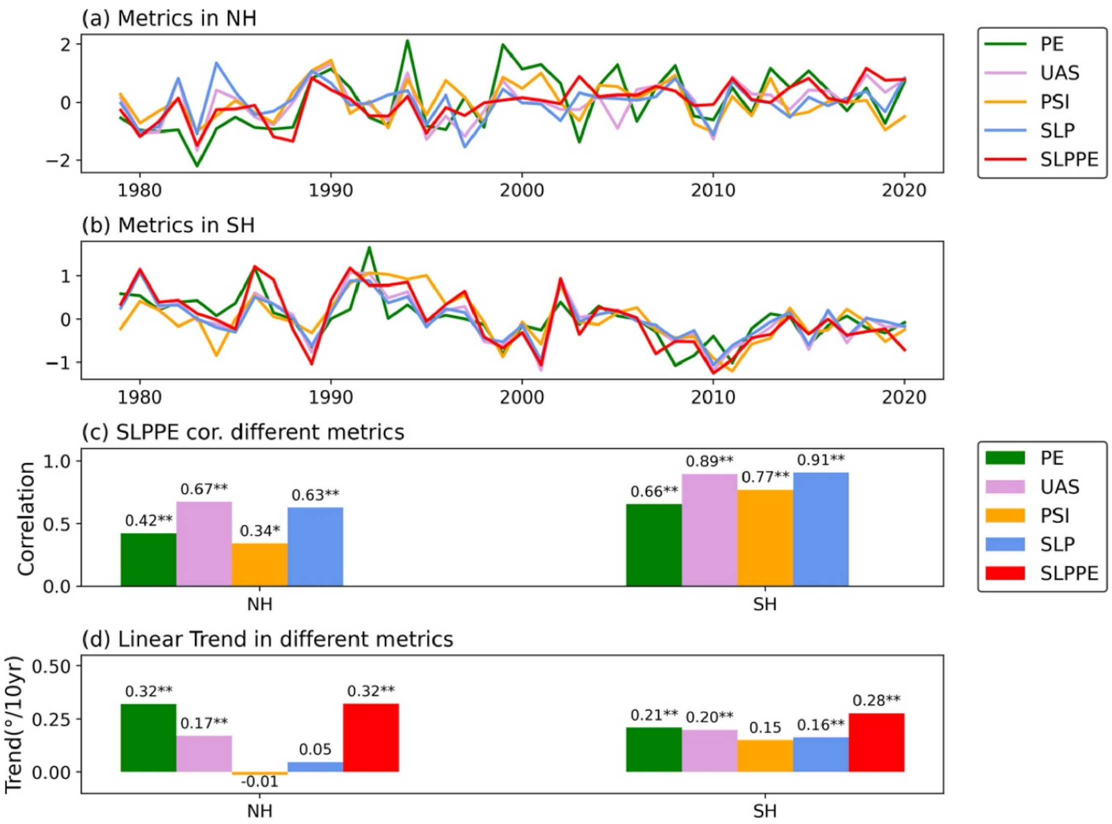

Figure 2. Time series of zonal mean positions of RTE based on SLPPE metric for the (a) NH and (b) SH, along with the time series of positions of tropical edge based on the four zonal mean metrics based on PSI, PE, SLP, and UAS. (c) Correlation coefficients of detrended time series of SLPPE metric with those of the other four metrics in the NH and SH. (d) Linear trends (degrees/decade, poleward positive) of the time series of the five metrics in the NH and SH. ** denotes significance at the 99% confidence level, while * denotes significance at the 95% confidence level.

ERA5 (figures 3(a) and S4), demonstrating that there is no data dependency in the results.

3.3. Interaction with the climate modes

The expansion of the zonal mean tropical edge is typically influenced by climate modes, such as the Pacific Decadal Oscillation (PDO; Grassi *et al* 2012, Allen *et al* 2014, Brönnimann *et al* 2015, Amaya *et al* 2017), the Atlantic Multi-decadal Oscillation (AMO; Brönnimann *et al* 2015, Cao *et al* 2020), the El Niño-Southern Oscillation (ENSO; Lu *et al* 2008, Feng and Li 2013, Nguyen *et al* 2013, Adam *et al* 2014, Rollings and Merlis 2021, Li *et al* 2023b), the Arctic oscillation (AO; Hu *et al* 2019, Moon and Ha 2019), the Southern Annular Mode (SAM; Previdi and Liepert 2007, Son *et al* 2009, Polvani *et al* 2011a, 2011b, Min and Son 2013, Lucas and Nguyen 2015). These modes are also recognized as drivers of RTE change, with their own distinct geographical contributions. Besides, the North Atlantic Oscillation (NAO) and the Pacific–North American teleconnection (PNA) have the potential contributions to RTE change, as that they have significant variability and are important to regional climate (Loon and Rogers 1978, Horel and Wallace 1981, Hoerling *et al* 1997, Wang *et al* 2021, 2023, Li *et al* 2023a). To better understand their complex interplay, the global RTE are divided into 12 regions with six regions in each hemisphere according to the regional feature of inter-annual variability and long-term trend in section 3.2, and their interaction with the seven climate modes and the significant results are summarized in figure 4. The 12 regions are shown as 12 boxes in figure 4, including North Africa (10° W–50° E), Central Asia (50° E–85° E), East Asia (85° E–125° E), North Pacific (125° E–120° W), North America (120° W–80° W), and North Atlantic (80° W–10° W) in the NH, as well as South Africa (15° E–40° E), South India Ocean (40° E–110° E), Australia (110° E–180°), South Pacific (180°–80° W), South America (80° W–40° W), and South Atlantic (30° W–10° E) in the SH. Seven climate modes mentioned above are chosen, ensuring a comprehensive representation of major global climate variabilities and considering their importance to contribute RTE change. The sources of the seven modes are listed in supplemental table S1. The instantaneous states of the seven climate modes are represented by a monthly index, and then the annual average of each mode is calculated to obtain the yearly time series.

Partial correlations are used to measure the linear relationships between each climate mode and

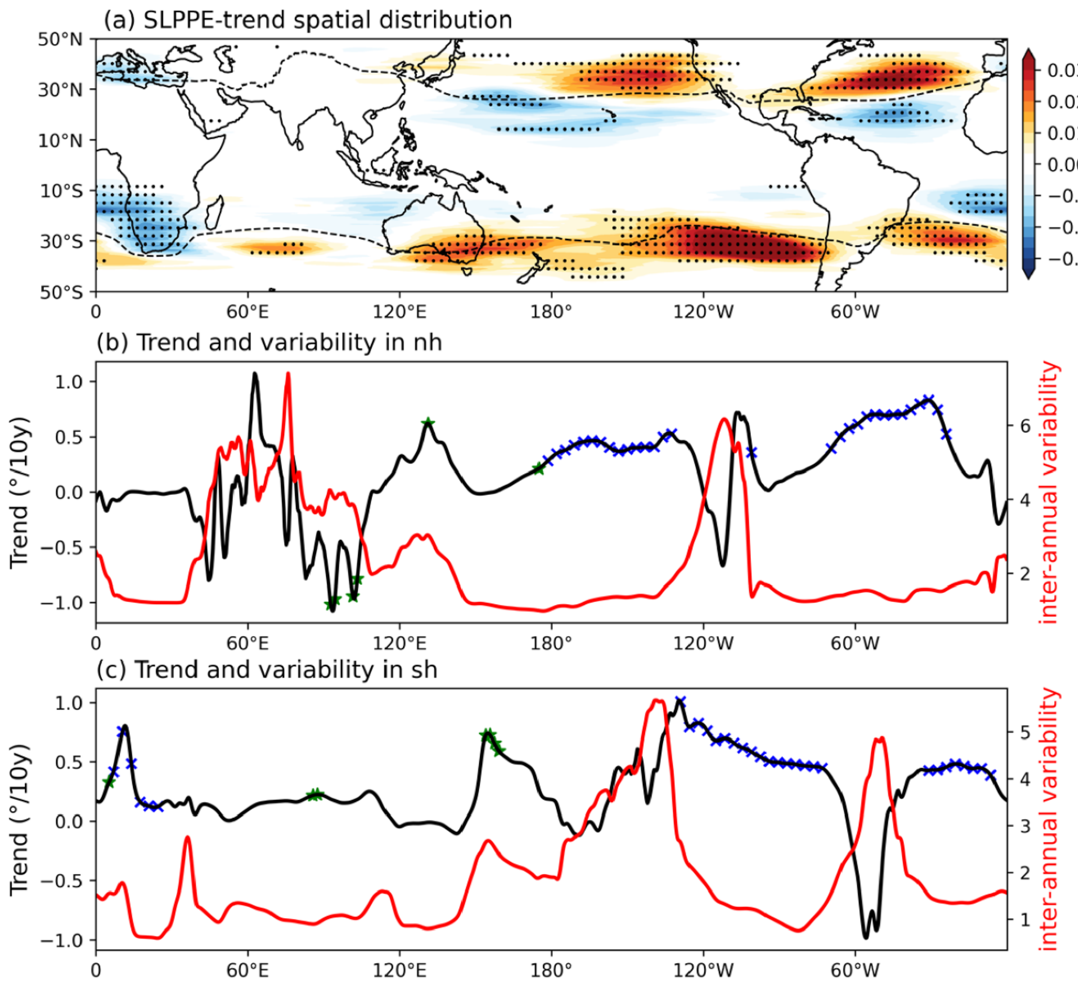

Figure 3. (a) Spatial distribution illustrating the linear trend of joint CDF between SLP and PE (shaded), with the black dashed line denoting the location of the climatological maximum joint CDF between SLP and PE. (b) Linear trends (black line, degrees/decade, poleward positive) and inter-annual variations (red line) of the RTE in the NH. (c) Same as (b) but in SH. Dots in (a) and blue crosses in (b) and (c) denote significance at the 95% confidence level, and green stars in (b) and (c) denote significance at the 90% confidence level.

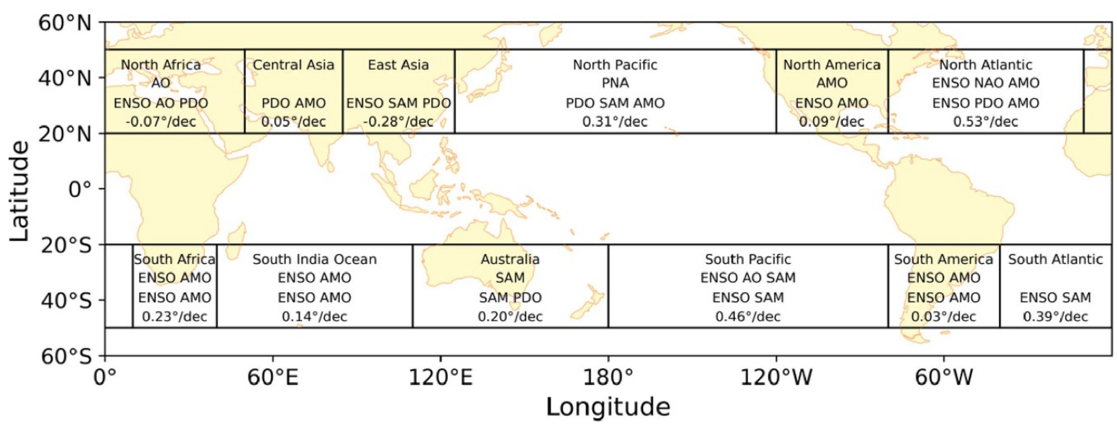

Figure 4. Summary of the relationship between climate modes and RTE. The first, second, third, and forth line in each box denote the name of the region, major inter-annual influencing factors, major long-term contribution factors, and RTE expansion rates, respectively.

RTE by isolating the covariance among the seven modes. Meanwhile, partial regression can be used to assess the congruent part of the contribution of each climate mode to RTE trends by multiplying the partial regression coefficients and trends of each mode (Thompson *et al* 2000, Ma and Zhou 2016, Hu *et al* 2020), which can be normalized by original RTE trends to obtain the relative contribution percentage.

The partial correlation coefficients between the seven climate mode indices and RTE locations over the six regions in the NH and SH are summarized in supplemental tables S2 and S3, respectively. In the NH, the ENSO, PNA, NAO, AO, and AMO emerge as prominent contributors, exerting substantial influence over multiple geographical regions (table S2 in the supplemental material). AMO has a noteworthy impact on the inter-annual variation of RTE over North America and the North Atlantic, and ENSO and NAO exert a pivotal role in the RTE over the North Atlantic with correlation coefficients at −0.36 and 0.38, respectively. Besides, the RTE over the North Pacific experiences a discernible effect from PNA, and AO highly correlates with the RTE over North Africa at 0.57.

In the SH, ENSO exhibits substantial impacts, particularly over regions such as South Africa, the Indian Ocean, and the South Pacific (table S3 in the supplemental material). AMO shows high correlation coefficient with the RTE over the South Indian Ocean, South America, and South Africa. Additionally, the influence of the SAM is paramount in shaping the climate patterns in the SH, with pronounced effects observed in the South Pacific and Australia. Note that although the correlation coefficient between AO and RTE over the South Pacific is significant, this relationship reflects rather than a case of direct 'cause and effect'. Certain regions, such as the South Atlantic and Central Asia, are not significantly influenced by the seven modes.

The contribution of seven climate modes to the trends of RTE locations over the six regions in the NH and SH are summarized in supplemental tables S4 and S5, respectively. In the NH, ENSO plays a crucial role in driving the expansion trends of the RTE, with substantial contributions from the six regions except the North Pacific (table S4 in the supplemental material). Although PDO does not exhibit significant inter-annual correlations with the RTE in most regions, it considerably contributes to the RTE expansion. It is particularly evident in the North Pacific and North Atlantic, where also experience the most significant expansion (figure 3(b)). Additionally, no less than 10% of RTE trends in the six regions are modulated by AMO, and AO's impact mainly appears over North Africa.

Similar to the SH, ENSO, PDO, and AMO exhibit pronounced contributions to RTE trends of most regions over the SH (table S5 in the supplemental material). SAM is another important climate mode, which largely influences the RTE trends over Australia, the South Pacific, and the South Atlantic. These findings indicate that the relationship between climate modes and RTE depends on the geographical location, and the SLPPE metric provides a more convenient way to investigate their regional connections.

4. Conclusion

In this study, the RTE are investigated with two appropriate variables: maximum SLP and minimum PE, which are combined to form a new metric under the multivariate probabilistic framework. This SLPPE metric effectively captures inter-annual variations and long-term trends in the zonal mean tropical edge. The zonal mean positions of RTE based on the SLPPE metric closely correlate with the positions of tropical edge based on PSI and UAS metric, with the correlation coefficient no less than 0.34. Besides, the poleward shifts of the tropical edge are observed both in the NH and SH, but their expansion rates are larger than those of PSI and UAS metric.

Furthermore, the SLPPE metric offers a flexible approach for capturing inter-annual variations and long-term trends of RTE locations at regional scale. In the NH, the significant poleward shifts of RTE over the North Pacific and North Atlantic are observed, and the strong inter-annual variability of RTE are located at most regions of Eurasia and North America. In the SH, pronounced poleward RTE trends were evident over the South Pacific, South Atlantic, and South Africa, and the inter-annual variations of RTE are vigorous over the part of the South Pacific and South America. Therefore, the pronounced RTE trends are primarily located over the oceanic regions, while the terrestrial areas exhibit more substantial inter-annual variability.

This study also investigates the relationship between climate modes and RTE from the inter-annual variations and long-term trends perspective. In the NH, ENSO and AMO exert widespread impacts across most regions on inter-annual variations and long-term trends of RTE, and PNA, NAO, and AO highlight the inter-annual relationship with RTE in the specific regions, as North Pacific, North Atlantic, and North Africa, respectively. In the SH, besides that ENSO and AMO wield notable influence over most regions on inter-annual variations and long-term trends of RTE, SAM also plays an important role in the RTE change around Australia and continuing eastward to the South Atlantic. Furthermore, the impacts of PDO on RTE are more inclined to long-term contribution rather than inter-annual relationship.

Note that although there is no benchmarking to directly measure the SLPPE metric's superiority and reliability, which are guaranteed in the present study by multiple reasons. Firstly, the selection of SLP and PE is grounded in a physical understanding to establish a robust link between the new metric and RTE. Secondly, the multivariate probabilistic framework enriches the relationship between variables, and avoids dependency of a single variable. Thirdly, the RTE obtained by SLPPE metric is continuous in zonal direction, and can captures the common features of climatology, inter-annual variations, and long-term trends of RTE based on the other single variable metrics in previous studies. By considering these aspects comprehensively, the SLPPE metric shows clear physical implication, and the conclusions by using the SLPPE metric are robust.

For the probabilistic framework in the present study, it innovatively offers the ability to use multiple variables to define the positions of RTE, and this method considers the physical relationship among multiple variables simultaneously, providing a valuable tool for climate change assessment studies involving model simulations. Besides, the annual positions of RTE are calculated based on the annual average of the two variables in the present study, and the same framework could be used for obtaining the monthly and seasonal positions of RTE crossing all longitudes to analyze their monthly and seasonal dynamics. All these will significantly contribute to the understanding of the Hadley circulation and its impacts on the associated regional climate.

Data availability statement

The ERA5 dataset can be accessed from www.ecmwf.int/en/forecasts/dataset/ecmwf-reanalysis-v5. The JRA-55 reanalysis dataset can be accessed from https://jra.kishou.go.jp/. The MERRA2 dataset is obtained from https://disc.gsfc.nasa.gov.

Acknowledgments

This work is supported by the National Natural Science Foundation of China (Grant Nos. 42141019, 42175049, 42261144687, and 42488201) and the Second Tibetan Plateau Scientific Expedition and Research (STEP) program (Grant No. 2019QZKK0102).

ORCID iDs

Xinxian Feng https://orcid.org/0000-0003-2441-1608
Weichen Tao https://orcid.org/0000-0002-4629-576X
Gang Huang https://orcid.org/0000-0002-8692-7856
Kaiming Hu https://orcid.org/0000-0002-9988-5747
Ya Wang https://orcid.org/0000-0003-1527-5413

References

Adam O, Grise K M, Staten P, Simpson I R, Davis S M, Davis N A, Waugh D W, Birner T and Ming A 2018 The TropD software package (v1): standardized methods for calculating tropical-width diagnostics *Geosci. Model Dev.* **11** 4339–57

Adam O, Schneider T and Harnik N 2014 Role of changes in mean temperatures versus temperature gradients in the recent widening of the Hadley circulation *J. Clim.* **27** 7450–61

Allan R P and Soden B J 2007 Large discrepancy between observed and simulated precipitation trends in the ascending and descending branches of the tropical circulation *Geophys. Res. Lett.* **34** L18705

Allen R J, Norris J R and Kovilakam M 2014 Influence of anthropogenic aerosols and the Pacific Decadal Oscillation on tropical belt width *Nat. Geosci.* **7** 270–4

Allen R J, Sherwood S C, Norris J R and Zender C S 2012 Recent Northern Hemisphere tropical expansion primarily driven by black carbon and tropospheric ozone *Nature* **485** 350

Amaya D J, Siler N, Xie S-P and Miller A J 2017 The interplay of internal and forced modes of Hadley cell expansion: lessons from the global warming hiatus *Clim. Dyn.* **51** 305–19

Anjana U and Kumar K K 2023 New insights into the poleward migration of tropical cyclones and its association with Hadley circulation *Sci. Rep.* **13** 15009

Archer C L and Caldeira K 2008 Historical trends in the jet streams *Geophys. Res. Lett.* **35** L08803

Baldassare D, Reichler T, Plink-Björklund P and Slawson J 2023 Large uncertainty in observed meridional stream function tropical expansion *EGUsphere* **2023** 1–24

Birner T, Davis S M and Seidel D J 2014 The changing width of Earth's tropical belt *Phys. Today* **67** 38–44

Brönnimann S, Fischer A M, Rozanov E, Poli P, Compo G P and Sardeshmukh P D 2015 Southward shift of the northern tropical belt from 1945 to 1980 *Nat. Geosci.* **8** 969–74

Cai W, Cowan T and Thatcher M 2012 Rainfall reductions over Southern Hemisphere semi-arid regions: the role of subtropical dry zone expansion *Sci. Rep.* **2** 702

Cao Y, Liang S and Yu M 2020 Observed low-frequency linkage between Northern Hemisphere tropical expansion and polar vortex weakening from 1979 to 2012 *Atmos. Res.* **243** 105034

Chen S, Wei K, Chen W and Song L 2014 Regional changes in the annual mean Hadley circulation in recent decades *J. Geophys. Res. Atmos.* **119** 7815–32

Choi J, Son S-W, Lu J and Min S-K 2014 Further observational evidence of Hadley cell widening in the Southern Hemisphere *Geophys. Res. Lett.* **41** 2590–7

Dabang J and Huijun W 2005 Natural interdecadal weakening of East Asian summer monsoon in the late 20th century *Chin. Sci. Bull.* **50** 1923

Dai A 2011 Drought under global warming: a review *WIREs Clim. Change* **2** 45–65

Davis N A and Davis S M 2018 Reconciling Hadley cell expansion trend estimates in reanalyses *Geophys. Res. Lett.* **45** 11439–46

Davis N and Birner T 2017 On the discrepancies in tropical belt expansion between reanalyses and climate models and among tropical belt width metrics *J. Clim.* **30** 1211–31

Davis S M and Rosenlof K H 2012 A multidiagnostic intercomparison of tropical-width time series using reanalyses and satellite observations *J. Clim.* **25** 1061–78

Feng J and Li J 2013 Contrasting impacts of two types of ENSO on the boreal spring Hadley circulation *J. Clim.* **26** 4773–89

Feng S and Fu Q 2013 Expansion of global drylands under a warming climate *Atmos. Chem. Phys.* **13** 10081–94

Fu Q, Johanson C M, Wallace J M and Reichler T 2006 Enhanced mid-latitude tropospheric warming in satellite measurements *Science* **312** 1179

Fu Q and Lin P 2011 Poleward shift of subtropical jets inferred from satellite-observed lower-stratospheric temperatures *J. Clim.* **24** 5597–603

Gelaro R *et al* 2017 The modern-era retrospective analysis for research and applications, version 2 (MERRA-2) *J. Clim.* **30** 5419–54

Grassi B, Redaelli G, Canziani P O and Visconti G 2012 Effects of the PDO phase on the tropical belt width *J. Clim.* **25** 3282–90

Grise K M *et al* 2019 Recent tropical expansion: natural variability or forced response? *J. Clim.* **32** 1551–71

Grise K M and Davis S M 2020 Hadley cell expansion in CMIP6 models *Atmos. Chem. Phys.* **20** 5249–68

Grise K M, Davis S M, Staten P W and Adam O 2018 Regional and seasonal characteristics of the recent expansion of the tropics *J. Clim.* **31** 6839–56

He J and Soden B J 2016 A re-examination of the projected subtropical precipitation decline *Nat. Clim. Change* **7** 53

Hersbach H *et al* 2020 The ERA5 global reanalysis *Q. J. R. Meteorol. Soc.* **146** 1999–2049

Hoerling M P, Kumar A and Zhong M 1997 El Niño, La Niña, and the nonlinearity of their teleconnections *J. Clim.* **10** 1769–86

Horel J D and Wallace J M 1981 Planetary-scale atmospheric phenomena associated with the Southern Oscillation *Mon. Weather Rev.* **109** 813–29

Hoskins B J and Yang G-Y 2021 The detailed dynamics of the Hadley cell. Part II: December–February *J. Clim.* **34** 805–23

Hoskins B J, Yang G-Y and Fonseca R M 2020 The detailed dynamics of the June–August Hadley cell *Q. J. R. Meteorol. Soc.* **146** 557–75

Hu D, Guo Y-P, Tan Z-M and Guan Z 2019 Interannual relationship between the boreal spring Arctic oscillation and the Northern Hemisphere Hadley circulation extent *J. Clim.* **32** 4395–408

Hu K, Liu Y, Huang G, He Z and Long S-M 2020 Contributions to the interannual summer rainfall variability in the mountainous area of central China and their decadal changes *Adv. Atmos. Sci.* **37** 259–68

Hu Y and Fu Q 2007 Observed poleward expansion of the Hadley circulation since 1979 *Atmos. Chem. Phys.* **7** 5229–36

Hu Y, Huang H and Zhou C 2018 Widening and weakening of the Hadley circulation under global warming *Sci. Bull.* **63** 640–4

Hu Y, Zhou C and Liu J 2010 Observational evidence for poleward expansion of the Hadley circulation *Adv. Atmos. Sci.* **28** 33–44

Huang J *et al* 2017 Dryland climate change: recent progress and challenges *Rev. Geophys.* **55** 719–78

Huang J, Yu H, Guan X, Wang G and Guo R 2016 Accelerated dryland expansion under climate change *Nat. Clim. Change* **6** 166–71

Kang S M and Polvani L M 2011 The interannual relationship between the latitude of the eddy-driven jet and the edge of the Hadley cell *J. Clim.* **24** 563–8

Keyser D, Schmidt B D and Duffy D G 1989 A technique for representing three-dimensional vertical circulations in baroclinic disturbances *Mon. Weather Rev.* **117** 2463–94

Kobayashi S *et al* 2015 The JRA-55 reanalysis: general specifications and basic characteristics *J. Meteorol. Soc. Japan* II **93** 5–48

Kossin J P, Emanuel K A and Vecchi G A 2014 The poleward migration of the location of tropical cyclone maximum intensity *Nature* **509** 349–52

Lau W K M and Kim K-M 2015 Robust Hadley circulation changes and increasing global dryness due to CO_2 warming from CMIP5 model projections *Proc. Natl Acad. Sci.* **112** 3630–5

Lau W K M and Tao W 2020 Precipitation–radiation–circulation feedback processes associated with structural changes of the ITCZ in a warming climate during 1980–2014: an observational portrayal *J. Clim.* **33** 8737–49

Li G, Chen L and Lu B 2023a A physics-based empirical model for the seasonal prediction of the central China July precipitation *Geophys. Res. Lett.* **50** e2022GL101463

Li Y, Xie S P, Lian T, Zhang G, Feng J, Ma J, Peng Q, Wang W, Hou Y and Li X 2023b Interannual variability of regional Hadley circulation and El Niño interaction *Geophys. Res. Lett.* **50** e2022GL102016

Loon H V and Rogers J C 1978 The seesaw in winter temperatures between Greenland and Northern Europe. Part I: general description *Mon. Weather Rev.* **106** 296–310

Lu J, Chen G and Frierson D M W 2008 Response of the zonal mean atmospheric circulation to El Niño versus global warming *J. Clim.* **21** 5835–51

Lucas C and Nguyen H 2015 Regional characteristics of tropical expansion and the role of climate variability *J. Geophys. Res. Atmos.* **120** 6809–24

Ma J, Chadwick R, Seo K-H, Dong C, Huang G, Foltz G R and Jiang J H 2018 Responses of the tropical atmospheric circulation to climate change and connection to the hydrological cycle *Annu. Rev. Earth Planet. Sci.* **46** 549–80

Ma S and Zhou T 2016 Robust strengthening and westward shift of the tropical Pacific Walker circulation during 1979–2012: a comparison of 7 sets of reanalysis data and 26 CMIP5 models *J. Clim.* **29** 3097–118

Mamalakis A and Foufoula-Georgiou E 2018 A multivariate probabilistic framework for tracking the intertropical convergence zone: analysis of recent climatology and past trends *Geophys. Res. Lett.* **45** 13080–9

Mamalakis A, Randerson J T, Yu J-Y, Pritchard M S, Magnusdottir G, Smyth P, Levine P A, Yu S and Foufoula-Georgiou E 2021 Zonally contrasting shifts of the tropical rain belt in response to climate change *Nat. Clim. Change* **11** 143–51

Min S-K and Son S-W 2013 Multimodel attribution of the Southern Hemisphere Hadley cell widening: major role of ozone depletion *J. Geophys. Res. Atmos.* **118** 3007–15

Moon H and Ha K-J 2019 Distinguishing changes in the Hadley circulation edge *Theor. Appl. Climatol.* **139** 1007–17

Nguyen H, Evans A, Lucas C, Smith I and Timbal B 2013 The Hadley circulation in reanalyses: climatology, variability, and change *J. Clim.* **26** 3357–76

Nguyen H, Hendon H H, Lim E P, Boschat G, Maloney E and Timbal B 2017 Variability of the extent of the Hadley circulation in the southern hemisphere: a regional perspective *Clim. Dyn.* **50** 129–42

Polvani L M, Previdi M and Deser C 2011a Large cancellation, due to ozone recovery, of future Southern Hemisphere atmospheric circulation trends *Geophys. Res. Lett.* **38** n/a

Polvani L M, Waugh D W, Correa G J P and Son S-W 2011b Stratospheric ozone depletion: the main driver of twentieth-century atmospheric circulation changes in the Southern Hemisphere *J. Clim.* **24** 795–812

Previdi M and Liepert B G 2007 Annular modes and Hadley cell expansion under global warming *Geophys. Res. Lett.* **34** L22701

Rollings M and Merlis T M 2021 The observed relationship between Pacific SST variability and Hadley cell extent trends in reanalyses *J. Clim.* **34** 2511–27

Rykaczewski R R, Dunne J P, Sydeman W J, García-Reyes M, Black B A and Bograd S J 2015 Poleward displacement of coastal upwelling-favorable winds in the ocean's eastern boundary currents through the 21st century *Geophys. Res. Lett.* **42** 6424–31

Schmidt D F and Grise K M 2017 The response of local precipitation and sea level pressure to Hadley cell expansion *Geophys. Res. Lett.* **44** 10573–82

Schneider T 2006 The general circulation of the atmosphere *Annu. Rev. Earth Planet. Sci.* **34** 655–88

Schwendike J, Berry G J, Reeder M J, Jakob C, Govekar P and Wardle R 2015 Trends in the local Hadley and local Walker circulations *J. Geophys. Res. Atmos.* **120** 7599–618

Seidel D J, Fu Q, Randel W J and Reichler T J 2007 Widening of the tropical belt in a changing climate *Nat. Geosci.* **1** 21

Seidel D J and Randel W J 2007 Recent widening of the tropical belt: evidence from tropopause observations *J. Geophys. Res. Atmos.* **112** D20113

Seth A, Giannini A, Rojas M, Rauscher S A, Bordoni S, Singh D and Camargo S J 2019 Monsoon responses to climate changes—connecting past, present and future *Curr. Clim. Change Rep.* **5** 63–79

Sharmila S and Walsh K J E 2018 Recent poleward shift of tropical cyclone formation linked to Hadley cell expansion *Nat. Clim. Change* **8** 730–6

Solomon A, Polvani L M, Waugh D W and Davis S M 2016 Contrasting upper and lower atmospheric metrics of tropical expansion in the Southern Hemisphere *Geophys. Res. Lett.* **43** 10496–503

Son S-W, Tandon N F, Polvani L M and Waugh D W 2009 Ozone hole and Southern Hemisphere climate change *Geophys. Res. Lett.* **36** L15705

Stachnik J P and Schumacher C 2011 A comparison of the Hadley circulation in modern reanalyses *J. Geophys. Res. Atmos.* **116** n/a

Staten P W *et al* 2020 Tropical widening: from global variations to regional impacts *Bull. Am. Meteorol. Soc.* **101** E897–904

Staten P W, Grise K M, Davis S M, Karnauskas K and Davis N 2019 Regional widening of tropical overturning: forced change, natural variability, and recent trends *J. Geophys. Res. Atmos.* **124** 6104–19

Staten P W, Lu J, Grise K M, Davis S M and Birner T 2018 Re-examining tropical expansion *Nat. Clim. Change* **8** 768–75

Studholme J and Gulev S 2018 Concurrent changes to Hadley circulation and the meridional distribution of tropical cyclones *J. Clim.* **31** 4367–89

Thompson D W J, Wallace J M and Hegerl G C 2000 Annular modes in the extratropical circulation. Part II: trends *J. Clim.* **13** 1018–36

Tivig M, Grützun V, John V O and Buehler S A 2020 Trends in upper-tropospheric humidity: expansion of the subtropical dry zones? *J. Clim.* **33** 2149–61

Totz S, Petri S, Lehmann J and Coumou D 2018 Regional changes in the mean position and variability of the tropical edge *Geophys. Res. Lett.* **45** 12076–84

Wang L, Chen W, Huang G and Zeng G 2016 Changes of the transitional climate zone in East Asia: past and future *Clim. Dyn.* **49** 1463–77

Wang Y, Hu K, Huang G and Tao W 2021 Asymmetric impacts of El Niño and La Niña on the Pacific–North American teleconnection pattern: the role of subtropical jet stream *Environ. Res. Lett.* **16** 114040

Wang Y, Hu K, Huang G and Tao W 2023 The role of nonlinear energy advection in forming asymmetric structure of ENSO teleconnections over the North Pacific and North America *Geophys. Res. Lett.* **50** e2023GL105277

Waugh D W *et al* 2018 Revisiting the relationship among metrics of tropical expansion *J. Clim.* **31** 7565–81

Xian T and Homeyer C R 2019 Global tropopause altitudes in radiosondes and reanalyses *Atmos. Chem. Phys.* **19** 5661–78

Zhang L, Lau W, Tao W and Li Z 2020 Large wildfires in the Western United States exacerbated by tropospheric drying linked to a multi-decadal trend in the expansion of the Hadley circulation *Geophys. Res. Lett.* **47** e2020GL087911

Zhang L and Zhou T 2015 Drought over East Asia: a review *J. Clim.* **28** 3375–99